Aeolian Research 16 (2015) 55-68

http://dx.doi.org/10.1016/j.aeolia.2014.11.002

An empirical equation to estimate mineral dust concentrations from visibility observations in Northern Africa

C. Camino [a,b,⇑], E. Cuevas [a], S. Basart [c], S. Alonso-Pérez [a,d,e], J.M. Baldasano [c,f], E. Terradellas [g], B. Marticorena [h], S. Rodríguez [a], A. Berjón [a]

[a] Izaña Atmospheric Research Center, AEMET, Santa Cruz de Tenerife, Spain
[b] Technical University of Catalonia, Barcelona, Spain
[c] Earth Sciences Department, Barcelona Supercomputing Center-Centro Nacional de Supercomputación (BSC-CNS), Barcelona, Spain
[d] Institute of Environmental Assessment and Water Research (CSIC), Barcelona, Spain
[e] Universidad Europea de Canarias, Laureate International Universities, La Orotava, Spain
[f] Environmental Modeling Laboratory, Technical University of Catalonia, Barcelona, Spain
[g] SDS WAS Regional Center, AEMET, Barcelona, Spain
[h] LISA, UMR7583, CNRS, Universités Paris Est-Paris Diderot, Créteil, France

Abstract

This paper presents a new empirical equation relating horizontal visibility and PM_{10} dust concentrations. The new empirical equation (IZO-Eq) is derived from observations performed at the Izaña Atmospheric Observatory (IZO, 28.30ºN, 16.49ºW, 2367 m a.s.l., Tenerife, Spain), recorded during Saharan dust outbreaks from 2003 to 2010. A filter based on relative humidity, present-weather and aerosol optical properties is applied to identify dust events. IZO-Eq is validated in the Sahel region during the dry and wet seasons (2006-2008) using data from two PM_{10} monitoring stations from the African Monsoon Multidisciplinary Analysis (AMMA) International project, and data from the nearest meteorological synoptic stations. The estimated PM_{10} derived from IZO-Eq is compared against that those obtained by other empirical equations and dust surface concentrations from NMMB/BSC-Dust model. IZO-Eq presents better performance than the other equations in both dry and wet seasons when compared with observed PM_{10} at two Sahelian sites. IZO-Eq is also able to reproduce the surface concentration variability simulated by NMMB/BSC-Dust. Above 10 km of horizontal visibility, empirical equations cannot be used to estimate PM_{10}, since above this threshold equations estimate a nearly constant PM_{10} value, regardless of the visibility range. A comparison between the PM_{10} spatial distributions derived from visibility SYNOP observations through IZO-Eq, the modelled values from the NMMB/BSC-Dust model and aerosol optical depth (AOD) retrieved from MODIS is performed for the 2006-2008 period. The different spatial distributions present a rather good agreement among them as well as to reproduce the characteristic seasonal dust features over North Africa.

Keywords: PM_{10}, visibility, mineral dust, dust transport model, MODIS-AQUA

1. Introduction

Mineral dust has a strong interaction with the climate system through direct and indirect impacts (*IPCC, 2007, 2014)*. Directly, mineral dust influences the Earth's radiative budget by affecting the processes of absorption and scattering of solar and infrared radiation (*Tegen 2003; Perez et al. 2006; Balkanski et al. 2007; Heinold et al., 2008*) and indirectly, it affects the clouds condensation nuclei (*Hoose et al. 2008*) and ice nuclei (*Klein et al., 2010*), optical properties and lifetime of clouds, causing an indirect radiative forcing (*Ramanathan et al. 2001; IPCC, 2007)*. Mineral dust can be transported in large plumes many thousands of kilometers away from their source regions causing changes in the biogeochemical processes of terrestrial and marine ecosystems (*Maher et al. 2010*) and, being an important source of primary nutrients such as nitrogen, phosphorus or potassium (*Jinkells, 2005*).

Mineral dust emissions into the atmosphere have a negative impact on human health, causing or aggravating allergies, respiratory diseases and eyes infections *(Griffin and Kellogg, 2004, WHO, 2005)*. During Saharan dust intrusions in Spain, *Díaz et al.* (2012) observed effects of PM_{10} (mass concentration of particulate matter with aerodynamical diameter less than 10 μm) on mortality due to respiratory causes in the cold season and to circulatory causes in the warm one. *Griffin (2007)* summarized the current state of knowledge of desert dust microbiology and the health impact that desert dust and its microbial constituents may have on downwind environments, both close and far from their sources. Saharan dust seems to be related with meningitis epidemics in the Sahel region (*Thomson et al. 2006, Cuevas et al. 2011, Pérez et al. 2014*) and increased incidence of pediatric asthma crisis in the Caribbean region *(Gyan et al. 2005*). *Stefanski and Sivakumar (2009)* summarized the negative impacts of sand and dust storms on agriculture. High dust concentrations increase significantly light extinction affecting negatively aircraft operations and ground transportation. *Ohde and Siegel (2012)* and *Schroedter-Homscheidt et al. (2012*) assessed the impact of Saharan dust on solar irradiance in concentrated photovoltaic plants.

There is an increasing interest in quantifying the mineral dust concentration over North Africa, which is the most important dust source of the world (*Prospero et al. 2002; Washington et al., 2003; Shao et al. 2011; Ginoux et al., 2012, Hsu et al., 2012*). However, air quality monitoring stations in rural sites or near dust sources over Northern Africa are almost inexistent. A variety of global and regional dust models have been used to characterize the dust cycle over main source regions (*Nickovic et al., 2001; Morcrette et al. 2009; Pérez et al. 2011*), but there are significant differences in the results among models (*Uno et al., 2006; Todd et al., 2008; Huneeus et al. 2011*). Satellite remote sensing has been used for dust detection, but the high reflectivity of the desert ground in the visible channels supposes a severe limitation to retrieve quantitative aerosol data from satellite (*Hsu et al. 2004; de Paepe and Dewitte 2009*). The AErosol RObotic NETwork, (AERONET, *Holben et al. 1998*) has also been used to derive dust content in the atmospheric column and to characterize the optical properties of mineral dust near source regions. However, AERONET observations are very scarce in- near- dust source regions, and the available time series are relatively short, presenting many gaps. It is worthily to note that column aerosol data often do not have a clear correspondence with surface concentration. Moreover, such measurements integrate different types of particles.

In order to overcome this strong observational limitation, horizontal visibility obtained from meteorological reports (SYNOP) has been used to infer surface dust concentration (*D'Almeida, 1986; Ben Mohamed et al. 1992; Ozer et al. 2006; Mahowald et al. 2007; Dayan et al. 2008*). The horizontal visibility is an indication of the intensity of attenuation of solar radiation by the suspended particles (*N'Tchayi et al., 1997*). It is strongly influenced by dust particle size distribution (*Tegen et al. 2003 Mahowald et al., 2013*) and also has a clear dependence on the ambient humidity (*Shao et al. 2006; Cabello et al. 2012*). However, many studies have shown that horizontal visibility is a good indicator of dust storms (*e.g N'Tchayi et al., 1997; Shao et al.,2003; Shao et al., 2006; Mahowald et al., 2007; Klose et al. 2010; Hamidi et al., 2014*). Several empirical equations relating surface dust concentrations and visibility have been proposed in dust regions, such as North America (*Chepil and Woodruff, 1957; Patterson and Gillete, 1977*), Australia (*Tews, 1996; Leys et al. 2002),* Asia (*Shao et al. 2003; Wang et al. 2008, Jugder et al., 2014*), West Asia (*Dayan et al. 2008*) and in West Africa (*D'Almeida, 1986; Ben Mohamed et al. 1992*).

In the present study we propose a new empirical equation relating horizontal visibility and PM_{10} using high quality data obtained at the high-mountain Izaña Global Atmospheric Watch (GAW) observatory (IZO, Tenerife, The Canary Islands), located at the subtropical eastern North Atlantic, near Africa and under environmental conditions ensuring that practically all PM_{10} recorded corresponds to mineral dust coming from the Sahara. Results are validated through the comparison of independent in-situ measurements at two PM_{10} stations located in the Sahel with visibility observations, with surface dust concentration from the NMMB/BSC-Dust model and with PM_{10} estimations from other referenced empirical equations derived for West Africa, Middle East and East Asia.

The paper is structured as follows: data and methods used to derive the empirical equation at IZO and to validate it over the Sahel region are described in Section 2, results are presented in Section 3, and in Section 4 the main conclusions are summarized.

2. Data and methods

2.1 PM_{10} and TSP

The present analysis includes PM_{10} and Total Suspended Particles (TSP) ($\mu g/m^3$) measured at IZO (28.30ºN, 16.49ºW, 2,367 m a.s.l.,) during the period spanning from January 2003 to January 2010. IZO station is managed by the Izaña Atmospheric Research Center (IARC), from the Meteorological State Agency of Spain (AEMET). Quasi-permanent subsidence conditions in the free troposphere together with frequent trade winds flow in the lowest troposphere resulting in a strong and stable temperature inversion (located at 1400m a.s.l. on average) that separates a dry free troposphere from a relatively fresh and humid oceanic boundary layer (Torres et al., 2002). Given its close proximity to the western Africa coast, IZO is an excellent site to study and characterize almost pure mineral dust released from African source regions and its transport over the subtropical North Atlantic (*Alonso-Pérez et al., 2007; 2011; Basart et al., 2009; Rodríguez et al., 2011*). Details of the methodology to determine PM_{10} and TSP mass concentrations at IZO station can be found in *Rodríguez et al. (2009; 2011; 2012).* Simultaneous PM_{10} measurements and visibility observations from 06 to 18 UTC

every 3 hours have been used to obtain daily means and to derive the empirical relationship between both parameters. Since some empirical equations considered in this paper use TSP instead of PM10, an averaged PM_{10}/TSP ratio has been computed from a set of simultaneous values of these variables.

The empirical equation obtained at IZO (IZO-Eq) has been validated using daily PM_{10} averages at two monitoring stations from the African Monsoon Multidisciplinary Analysis (AMMA) International Project (*Marticorena et al., 2010)* in the Sahel region from January 2006 to December 2008. The AMMA stations are M'Bour (Senegal, 14.39°N, 16.96°W, 13 m a.s.l.), located near the Atlantic coast and Banizoumbou (Niger, 13.54°N, 2.66°E, 191 m a.s.l.), representative of the inland Sahel. Both stations are aligned around the parallel of 14° N along the east-west Sahelian dust corridor (Figure 1). PM_{10} concentrations at the AMMA sites were measured using a Tapered Element Oscillating Microbalance (TEOM 1400A from Thermo Scientific) ambient air monitor with an acquisition time of 5 min (*Marticorena et al., 2010).*

TSP measurements taken at Banizoumbou station during AMMA field campaigns have been used to compute an averaged PM_{10}/TSP ratio representative for the Sahel region. The period for sampling TSP mass concentrations corresponds to Special Observing Periods (SOP) 0, 1 and 2 of the AMMA intensive field campaigns held from 12 January to 13 February, 2006 and from 1 June to 17 July 2006 (*Rajot et al. 2008; Lebel et al. 2010; Desboeufs et al. 2010*). The methodology used in the measurements can be found in *Rajot et al.* (2008).

2.2 Horizontal visibility and meteorological data

Horizontal visibility and meteorological data are retrieved from the BDM meteorological database created and maintained by AEMET. The three SYNOP stations located close to the PM_{10} monitoring stations that have been selected are IZO, Dakar (Senegal, 14.73ºN, 17.15ºW, 24 m a.s.l.) and Niamey (Niger, 13.48ºN, 2.17ºE, 227m a.s.l.) (Figure 1). Daily visibility values are obtained for Dakar and Niamey after averaging 3-hourly observations. In contrast, visibility observations coincident with measurements of mass concentration have been considered for IZO station.

Visibility data associated to the presence of hydrometeors, such as fog, mist or rain, are discarded using relative humidity (RH) and present weather as filters. On the one hand, observations with RH above 75% are not considered. On the other hand, the following values of present weather are used to identify those visibility observations whose reduction is only attributable to dust-related phenomena: 1) dust in suspension (SYNOP codes 05-06), 2) blowing dust (SYNOP code 07), 3) dust storm (SYNOP codes 09,30-32) and 4) severe dust storm (SYNOP codes 33-35 and 98). In addition, values of present weather denoting clear skies, clouds dissolving, state of sky unchanged, and clouds developing at the time of the observation (SYNOP codes 00-03; hereafter referred to clear sky conditions) are also considered.

2.3 AERONET data

In the derivation of the empirical equation at IZO station, sunphotometer data from a collocated AERONET site have been used to ensure visibility is exclusively reduced by the presence of mineral dust. However, in the Sahel region, AERONET data have been utilized only to assess the visibility, RH and present weather, statistics at each AMMA

station. The AERONET stations used in the present study are: IZO, Dakar (Senegal, 14.39ºN, 16.95ºW, 0 m a.s.l.) and Banizoumbou (Niger, 13.54ºN, 2.66ºW, 250 m a.s.l.) (Figure 1). Quality-assured AERONET data (Level 2.0) in the 440-870nm wavelength range are used to calculate the AOD at 550nm, from the Ångström's equation, and the Ångström exponent (AE). The contribution of fine and coarse particles is analyzed using the fine mode fraction, (FMF) retrieved with the spectral deconvolution algorithm (*O'Neill et al. 2003*). Only AERONET measurements within ± 30 min of visibility observations have been used. We assume that desert dust events correspond to AOD ≥ 0.15 and AE ≤ 0.75 (*Basart et al. 2009)*, and following *Toledano et al.* (2011), we establish the additional condition of FMF ≤ 0.30 to identify those cases with almost pure mineral dust.

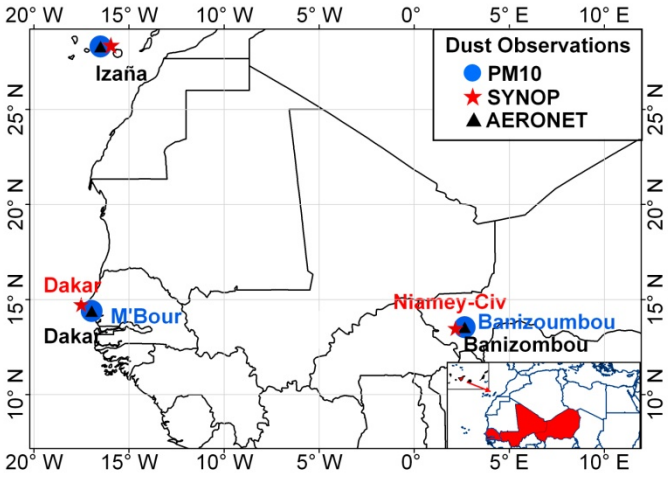

Figure 1*. Location of the PM_{10} monitoring sites (blue circles), meteorological stations (red starts) and AERONET stations (black triangles) near PM_{10} monitoring sites used in the present analysis.*

2.4 Comparison with other empirical equations

The empirical equation relating PM_{10} and horizontal visibility obtained at IZO has been compared with empirical equations derived by other authors within the broad "dust belt" area (*Prospero et al. 2002; Ginoux et al., 2012*) which extends from the west coast of Northern Africa, over the Middle East, Central and South Asia to China.

Particularly, in northern Africa, D'Almeida (1986) established a widely known and used empirical relationship between horizontal visibility and aerosol mass concentration (hereafter referred as DA-Eq). However, *D'Almeida* (1986) established this relationship indirectly using experimental measurements with sunphotometers, assuming that horizontal visibility and aerosol turbidity parameters are often related to each other. Turbidity data was collected for a period of two years (1981 and 1982) from a network of eleven stations located relatively close to the major Saharan dust sources identified by D'Almeida (1986). However, visibility is reported from selected stations located one or two days travel distance from the real source location. Surface PM_{10} concentrations measurements used to develop DA-Eq were performed during a field campaign held at Agadez (Niger) in January and February 1982. PM_{10} concentrations ranged between 30 and 700 $\mu g/m^3$, while the visibilities ranged from 200 m to 400 km during winter months. PM_{10} represents quite well the concentration of desert mineral dust because

Saharan dust size distributions exhibit a typical coarse mode diameter situated at about 3.5 μm, with an overall dust mean particle diameter of 1.5 μm (Sunnu et al., 2008).

Ben Mohamed et al. (1992) used horizontal visibility data varying from 100 meters to 20 kilometers in the synoptic station located at Niamey Airport (Niger), over a period of 17 months (from February 1986 to June 1987), and associated Total Suspended Particles (TSP) mineral dust mass concentration measurements in order to establish a relationship between the two parameters (hereafter referred as BM-Eq). However, TSP is a parameter that is not commonly used today to express the surface aerosol concentration, and *Ben Mohamed et al*. (1992) did not establish a procedure to separate the contribution of biomass burning aerosols, from that of desert mineral dust.

Other studies have analyzed relationships between visibility and particulate matter concentration in non-African regions. In West Asia, Dayan et al. (2008) developed a PM_{10}-visibility empirical equation (hereafter referred as DAY-Eq) using visibility data together with co-located measurements of PM_{10} dust concentration measured at the airport of Hazerim in northern Negev desert (Israel) for a period of three years (2001–2003). Dayan et al. (2008) used two criteria to select dust observations: visibility ≤5 km, and no weather phenomena, other than haze or dust, responsible for reduction in visibility.

Shao et al. (2003) obtained a relationship between visibility and TSP in East Asia (hereafter referred as SH-Eq). They obtained two empirical equations for visibility < 3.5 and ≥ 3.5 km, respectively, in the period March-May 2002 during northeast Asian dust events caused by low-pressure frontal systems, referred to as Mongolian cyclones. However, the impact of air moisture on visibility was not included and the uncertainties in the empirical coefficients might be large (Shao et al., 2003).

Jugder et al. (2014) obtained empirical equations relating visibility and PM_{10} at four dust monitoring sites located at Dalanzadgad, Sainshand and Zamyn-Uud in the Gobi Desert during the period from January 2009 to May 2013, and at Bayan Unjuul, a steppe zone of Mongolia, from April to May 2008 (hereafter referred as Ju-Eq). PM_{10} concentrations were obtained by using light scattering technique. Visibility observations were performed with automated Meteorological Optical Range (MOR) sensors, with a maximum measurement range of 20 km. Jugder et al. (2014) established a criterion based on PM_{10} concentrations to separate normal (≤ 50 $\mu g/m^3$) from hazy atmospheric conditions (≥ 50 $\mu g/m^3$).

These equations are summarized in Table 1.

***Table 1**. Empirical equations to estimate dust concentration (PM_{10} or TSP in $\mu g/m^3$) using visibility (V in km) obtained by several authors within the dust belt.*

Authors	Code	Empirical equation	Dust concentrations and visibility data reported fromSYNOP station	Analysis period to derive the empirical equation
D'Almeida (1986)	DA-Eq	$PM_{10} = 914.0\, V^{-0.73} + 19.03$	Turbidity network of eleven stations set up over the Sahara and the Sahelian belt.	From January 1981 to December 1982
			PM_{10} field campaign at Agadez (Niger) with visibility ranges from 0.2 to 40 km	January and February 1982
Ben Mohamed et al. (1992)	BM-Eq	$TSP = 1339.84\, V^{-.67}$	TSP field campaign at Niamey (Niger) with visibility ranges from 0.1 to 20 km.	From February 1986 to June 1987
Shao et al. (2003)	SH-Eq	$TSP = 3802.29\ V^{-0.84}; V < 3.5$ km $TSP = e^{-0.11V+7.62}; V \geq 3.5$ km	TSP measured at twelve monitoring sites located in China, Japan and Korea. Visibility data disaggregated in weak dust events and strong dust events.	March, April, and May 2002
Dayan et al. (2008)	DAY-Eq	$PM_{10} = -505\ln(V) + 2264$	PM_{10} monitoring site located at Negev Desert. Visibility ranges from 1 to 5 km at Hazerim airport (Israel).	From January 2001 to December 2003
Jugder et al. (2014)	JU-Eq	$PM_{10} = 485.67\, V^{-0.776}$	PM_{10} and visibility data were observed at Zamyn-Uud site in the Gobi desert. $PM_{10} \geq 50\ \mu g/m^3$ threshold was established for hazy atmospheric conditions. Visibility MOR sensors have a maximum measurement range of 20 km.	From January 2009 to May 2013

2.5 Mineral dust model

Daily mean dust surface concentrations (equivalent to PM_{10} concentrations) simulated by NMMB/BSC-Dust v1.0 model reanalysis 1979-2010 run (*Pérez et al. 2011; Haustein et al. 2012*) at the Barcelona Supercomputing Center-Centro Nacional de Supercomputación (BSC-CNS) have been compared with daily mean PM_{10} concentrations measured at the two AMMA stations and with PM_{10} estimated from visibility observations within the period 2006-2008. Daily-averaged values of surface dust concentration from 3-hourly model outputs interpolated at each AMMA station. The NMMB/BSC-Dust model (http://www.bsc.es/earth-sciences/mineral-dust/nmmbbsc-dust-forecast/model-description/) has been developed by the Earth Sciences Department of BSC-CNS in collaboration with, the National Center for Environmental Prediction (NOAA/NCEP), NASA Goddard Institute for Space Studies and the International Research Institute for Climate and Society (IRI). The domain of the reanalysis covers Northern Africa, the Arabian Peninsula and southern and central Europe (0˚ to 65˚N and 25˚W to 60˚ E). The resolution of the model has been set to 0.5° x 0.5° with 40 hybrid sigma-pressure model layers. The simulations are reinitialized every 24 hours with NCEP Reanalysis-2 pressure level data and GLDAS data for soil moisture and temperature with a spin-up of 12 hours. A detailed description of the NMMB/BSC-Dust model can be found in Pérez et al. (2011).

2.6 MODIS

Daily AOD retrievals from the MODerate resolution Imaging Spectrometer (MODIS; http://disc.sci.gsfc.nasa.gov/giovanni) travelling on-board the Aqua satellite have been used to compare with corresponding maps of PM_{10} estimated from visibility and surface dust concentrations simulated by the NMMB/BSC-Dust model over Northern Africa during the dry and wet seasons in the Sahel region (2006-2008). We used a combination of the AOD data retrieved using dark-target and deep blue (DB) algorithms. Daily level-3 products (collection 5.1), consisting of daily global gridded data of aerosol parameters at a resolution of 1º x 1º (~110 km) have been used. The dark-target aerosol algorithm retrieves AOD data over vegetated surfaces and dark-soil regions under clear-sky (non-cloudy), in which the surface reflectance in the visible (0.47 and 0.65 μm) and near infrared (2.1 μm) channels presents low values (Levy et al., 2010). The DB algorithm retrieves AOD over visibly bright surfaces by taking advantage of dark-surface properties at blue channels (0.412, 0.47 μm) and weak absorption of dust at the red channel (0.65 μm) (Hsu et al., 2004; Shi et al., 2013).

2.7 Statistical parameters

The mean bias (MB), the modified normalized mean bias (MNMB), the fractional gross error (FGE), the root mean square error (RMSE), and the Pearson correlation coefficient (r) have been used as skill scores to validate the performance of the empirical equations. The MB captures the average deviations between estimated and observed values. The MNMB is selected as it treats both model deficiencies (over- and underestimation with respect to observed values) in a symmetric manner. It is bounded by the values ±2. Similarly, FGE is a measure of the overall model error and is bounded by the values 0 and 2. The RMSE metric estimates the spread of the individual errors of each dataset. It is strongly dominated by the largest values, due to the squaring operation. Especially in cases where prominent outliers occur, the usefulness of RMSE is questionable and the interpretation becomes difficult. The correlation coefficient captures the degree of match between estimated and observed values. The statistical scores are summarized in Table 2. They are computed using daily mean values. Datasets from the Sahelian stations have been split into two periods: the dry season (from October to April 2006-2008) and the wet season (from May to September 2006-2008) in order to quantify the performance of each empirical equation and the dust PM_{10} concentrations simulated by the NMMB/BSC-Dust model in two different meteorological scenarios.

Table 2. *Statistical scores used for the validation of estimated PM_{10} from visibility with observed PM_{10} at IZO and AMMA stations, where n is the number of data used in the analysis, f_i is the estimated PM_{10} value for each empirical equation and obs_i is the observed PM_{10}.*

Statistics			
Score	**Equation**	**Range**	**Perfect score**
Mean bias (MB)	$\mathbf{MB = \frac{1}{n}\sum f_i - Obs_i}$	**$-\infty$ to $+\infty$**	**0**
Modified, normalized mean bias (MNMB)	$\mathbf{MNMB = \frac{2}{n}\sum \frac{f_i - Obs_i}{f_i + Obs_i}}$	**-2 to 2**	**0**

Fractional gross error (FGE)	$\mathbf{FGE} = \frac{\mathbf{2}}{\mathbf{n}}\sum\left\|\frac{\mathbf{f_i} - \mathbf{Obs_i}}{\mathbf{f_i} + \mathbf{Obs_i}}\right\|$	**0 to 2**	**0**
Root mean square error (RMSE)	$\mathbf{RMSE} = \sqrt{\frac{\mathbf{1}}{\mathbf{n}}\sum(\mathbf{f_i} - \mathbf{Obs_i})^2}$	**0 to + ∞**	**0**
Pearson correlation coefficient (r)	$\mathbf{r} = \frac{\frac{\mathbf{1}}{\mathbf{n}}\sum(\mathbf{f_i} - \bar{\mathbf{f}})(\mathbf{obs_i} - \overline{\mathbf{obs}})}{\boldsymbol{\sigma_f \sigma_{obs}}}$	**-1 to 1**	**1**

3. Results

3.1 Determination of the PM_{10} – visibility empirical equation

IZO is normally under free troposphere conditions. Thus, the AOD is usually low: approximately 85% of the background values are below 0.15 (*Basart et al., 2009*). Hence, a reduced number of hourly data pairs of PM_{10}-visibility observations are found when aerosol criteria to select dust events are applied (AOD $\geq$ 0.15, AE $\leq$ 0.75 and FMF $\leq$ 0.30).

Once no-dust cases are ruled out, daily means of PM_{10}, TSP and visibility are calculated from hourly observations. Most observations (83.87%) used to derive the empirical equation correspond to the summer season (July-September), when the major Saharan high-level dust intrusions are reported at IZO (Basart et al., 2009; *Rodriguez et al., 2011*). Another significant part (9.67%) corresponds to spring (March-June), when Saharan low-level dust intrusions over the Canary Islands occur (*Alonso-Pérez et al., 2007*). The best fit between visibility and PM_{10} concentrations is the following potential equation (r =0.68 and p-value $\leq$ 0.005):

$$\boldsymbol{PM_{10} = 1772.24\, V^{-1.1}} \qquad \textbf{(1)}$$

where V is the horizontal visibility in km. The empirical equation 1 (henceforth referred to as IZO-Eq) is obtained using a total of 93 daily pairs of observations (~5% of total PM10-visibility pairs in the period 2003-2010), in which daily PM_{10} means ranged between 10 and 315 μg/m^3 and daily visibility means ranged between 4 and 75 kilometers.

PM_{10} daily means versus visibility daily means recorded at IZO, and the best fits using different equations, are shown in Figure 2. The PM_{10}/TSP ratios ranged from 0.57 to 0.80, being 0.65±0.08 the overall mean ratio. Estimated TSP concentrations from BM-Eq and SH-Eq are converted to PM_{10} using the minimum, maximum and average value of the PM_{10}/TSP ratio found experimentally, in order to assess the impact of the PM_{10}/TSP ratio uncertainty on PM_{10} derived from these two equations. In the case of JU-Eq we have used the empirical relationship obtained at Zamyn-Uud station by Jugder et al. (2014), which showed the best agreement with the rest of the equations. DAY-Eq has not been analyzed at IZO station because it was derived for visibilities $\leq$ 5 km, a very low threshold for this station.

Figure 2*. Daily mean PM_{10} (μg/m^3) versus daily mean visibility (km) recorded at IZO (black dots). Best fit found at IZO (IZO-Eq), and estimated PM_{10} from DA-Eq, BM-Eq,*

and SH-Eq. The error bars represent ± σ of estimated PM_{10} using the IZO-Eq. Since BM-Eq and SH-Eq provide TSP, the estimated values are converted to PM_{10} using an averaged TSP/PM_{10} ratio of 0.65 obtained at IZO station.

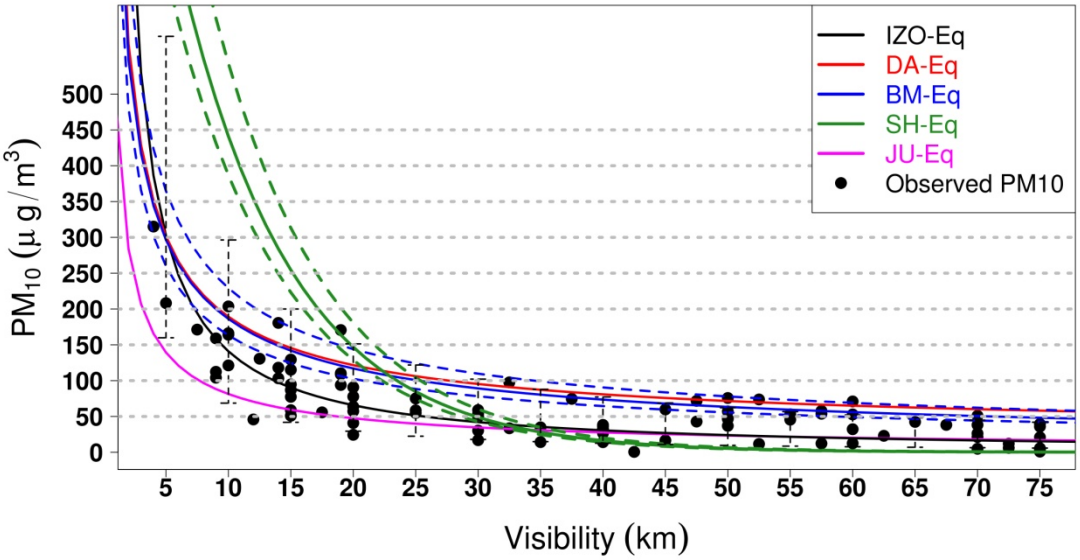

***Figure 2**. Daily mean PM_{10} (µg/m^3) versus daily mean visibility (km) recorded at IZO (black dots). Best fit found at IZO (IZO-Eq), and estimated PM_{10} from DA-Eq, BM-Eq, SH-Eq and JU-Eq. The error bars represent ± σ of estimated PM_{10} using the IZO-Eq. Since BM-Eq and SH-Eq provide TSP, the estimated values are converted to PM_{10} using an averaged TSP/PM_{10} ratio of 0.65 obtained at IZO station. These lines are confined within the dashed lines computed with the minimum (0.57) and maximum (0.80) PM_{10}/TSP values, respectively*

Basic descriptive statistics of observed and estimated PM_{10} for each empirical equation at IZO station are shown in Table 3. IZO-Eq provides the best scores. JU-Eq shows very similar basic statistics to IZO-Eq, and the same behavior as the latter for visibility > 20 km. DA-Eq and BM-Eq tend to overestimate, whereas SH-Eq shows a poor performance (Table 3, Figures 2 and 3). The highest differences respect the observed values are found for SH-Eq, probably because it was derived in Eastern Asia, where the occurrence of severe dust storms is more frequent than in the Canary Islands.

***Table 3**. Basic descriptive statistics of daily PM_{10} concentrations in µg/m^3 (mean, median, percentile 25th (P25) and 75th (P75), and RMSE) at IZO station for each empirical equation under dust conditions.*

	P25	Median	Mean	P75	RMSE
Observed PM_{10}	30	51	65	87	...
IZO-Eq	22	32	56	70	32
DA-Eq	68	82	104	127	50
BM-Eq * 0.57	52	66	86	106	36
BM-Eq * 0.65	**59**	**75**	**98**	**121**	**45**
BM-Eq * 0.80	73	92	120	149	67
SH-Eq * 0.57	4	18	118	159	142

SH-Eq * 0.65	**4**	**22**	**133**	**189**	**170**
SH-Eq * 0.80	4	26	157	223	224
JU-Eq	22	28	40	49	42

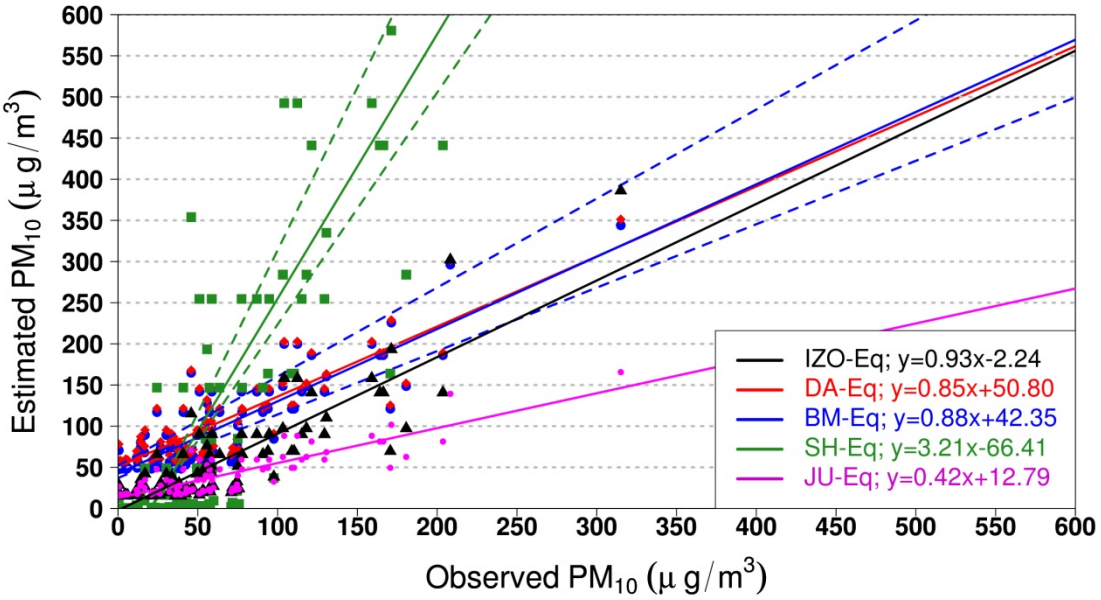

Figure 3*. Scatter plot of observed PM_{10} daily means versus estimated PM_{10} daily means at IZO station for IZO-Eq (black triangles), DA-Eq (red diamonds), BM-Eq (blue dots), SH-Eq (green squares), and JU-Eq (pink dots). The lines are the corresponding best fits of IZO-Eq (black), DA-Eq (red), BM-Eq (blue), SH-Eq (green), and JU-Eq (pink). Since BM-Eq and SH-Eq provide TSP, the estimated values are converted to PM_{10} using an averaged TSP/PM_{10} ratio of 0.65 obtained at IZO station. These lines are confined within the dashed lines computed with the minimum (0.57) and maximum (0.80) PM_{10}/TSP values, respectively*

3.2 Analysis of SYNOP observations over the Sahel region

In the Sahel region, most of highest daily PM_{10} concentrations are observed from October to April, that is during the dry season (*Yahi et al*. 2013), when the northeasterly trade winds (Harmattan winds) drive dust transport from the Saharan desert towards the Gulf of Guinea (*Prospero et al. 2002; Engelstaedter et al. 2006; Engelstaedter and Washington 2007; Marticorena et al. 2010; Formenti et al., 2011).* The minimum dust surface concentrations are recorded at AMMA stations during the wet season, from May to September, under the influence of the monsoon flow from South-West (*Flamant et al., 2007; Janicot et al., 2008; Flamant et al., 2009; Nicholson 2009; Marticorena et al. 2010; Desboeufs et al. 2010; Nicholson 2013*). The monsoon flow loaded with abundant humidity often produces intense rainfall in the Sahelian belt that inhibits local dust aerosol emission into the atmosphere and activates aerosol particles scavenging (*Engelstaedter and Washington 2007).* At the beginning of the monsoon season, before the growing vegetation, strong winds generated by mesoscale convective systems (MCS) raise large amounts of mineral dust into the atmosphere. Then, the strong updrafts associated to these meteorological systems transport the particles up to

altitudes favorable for long-range transport. (*Sterk, 2002; Flamant et al. 2007; Bou Karam et al. 2008; Flamant et al 2009; Bou Karam et al. 2009; Desboeufs et al. 2010*).

Meteorological reports from SYNOP stations that include present weather compatible with dusty conditions (clear sky conditions, dust in suspension and blowing dust) are analyzed during the dry and wet seasons together with PM_{10} and AERONET data from nearby stations. Daily data with RH above 75% or with reported precipitation are discarded. Dust storm and severe dust storm events have not been analyzed due to their low occurrence (≤ 0.05 %). The relative frequency of each present weather type and the average visibility, relative humidity and aerosols optical properties during the dry and wet seasons are shown in Table 4. Observations mostly correspond to clear conditions and dust in suspension, whereas blowing dust and dust storms occur with a very low frequency.

During the dry season, the average humidity is lower than 40%, as a consequence of the influence of the Harmattan winds, which increase the dust transport reducing the visibility. The relative humidity is lower in blowing dust conditions than in dust in suspension and clear sky conditions. The humidity is larger during the wet season for all present weather types due to the monsoon flow. The AOD is higher in the wet than in the dry season, whereas the AE and FMF are higher during the dry than in the wet season. It suggests a large contribution of coarse particles in the wet season as a consequence of the MCS activity. Although there is not a simple significant correspondence between visibility and AOD, which represents the vertically-integrated dust load, relatively high values of horizontal visibility have been often found with high AOD and low AE, suggesting that in the wet season the dust layer might be located in upper atmospheric levels. This agrees with results found by *Yahi et al.* (2013) when they compared surface dust concentration and AOD in the Sahel region during this season.

A striking result is the fact that the mean AOD values associated with reported clear skies conditions, although lower than those for dust conditions, are always higher than 0.33 in both seasons. Moreover, the highest average value of AE (0.46) associated with clear skies is lower than the threshold established by some authors to indicate that mineral dust is the dominant aerosol (i.e., *Basart et al., 2009*).). This suggests that SYNOP reports of clear sky often correspond to hazy atmospheric conditions, in which mineral dust might constitute the dominant aerosol fraction. On the other hand, during the dry season, clear-sky days present high values of AE and FMF. This indicates that the column aerosol content could be a mixture of mineral dust with finer aerosols, likely biomass burning, typical of winter months in the Sahel region (*Engelstaedter and Washington 2007; Rajot et al. 2008*).

Table 4*. Relative frequency (%) of clear sky conditions, dust in suspension, and blowing dust during the dry and wet seasons for the period 2006-2008, and averaged values of visibility, RH, AOD, AE and FMF.*

	(HR≤ 75, no Precipitation)	
	Dry season	**Wet season**
Clear sky conditions	**43.26 %**	**31.56 %**
AOD	0.33	0.49
AE	0.46	0.26
FMF	0.51	0.31
Visibility (km)	10.49	11.44

RH (%)	38	59
Dust in suspension	**20.26 %**	**1.75 %**
AOD	0.76	1.48
AE	0.26	0.14
FMF	0.40	0.35
Visibility (km)	4.45	4.70
RH (%)	25	48
Blowing dust	**0.71 %**	**0.25 %**
AOD	0.69	1.64
AE	0.17	0.002
FMF	0.33	0.15
Visibility (km)	3.34	5.00
RH (%)	13	45

3.3 Validation over the Sahel region

The performance of each empirical equation at the two AMMA stations and the NMMB/BSC-Dust model was quantified for both seasons with statistical scores. Hourly visibility observations corresponding to clear sky conditions, dust in suspension, blowing dust and dust storms were used to compute daily averages at each AMMA station. Results are summarized in Table 5 (dry season) and Table 6 (wet season). In case of DAY-Eq only those PM_{10}-visibility pairs corresponding to visibility range less than 5 km have been compared, since this empirical equation is only valid for visibility $\leq$ 5 km (*Dayan et al. 2008*). In order to compare TSP from BM-Eq and SH-Eq with PM_{10} observations, we used the minimum (0.60), maximum (0.98) and average value (0.80±0.09) of the PM_{10}/TSP ratio found experimentally at Banizoumbou station, similarly as was done for the equations intercomparison at IZO. The correlation coefficients between the observed PM_{10} in the AMMA sites and the PM_{10} obtained from IZO-Eq, DA-Eq, BM-Eq, SH-Eq and JU-Eq are $\geq$ 0. 78 for dry and wet season except for Banizoumbou at the dry season ($r > 0.40$) (see Tables 5 and 6). This indicates that, in general, the visibility database is able to reproduce the daily particulate matter concentration variability observed in the air quality stations.

Daily-mean values of PM_{10} and visibility under selected present weather types for each AMMA station and corresponding nearest SYNOP station during the dry and wet seasons for the period 2006-2008 are shown in Figure 4. The estimated PM_{10} from each empirical equation is also depicted. In Figures 5 and 6, the performance of IZO-Eq, DA-Eq and the NMMB/BSC-Dust model at each AMMA station is shown with estimated-observed PM_{10} daily means scatter plots for the wet and dry seasons, respectively. In general, the empirical equations overestimate PM_{10}, especially the SH-Eq because it was developed under severe dust storms during the spring season, exceeding in most of the cases four orders of magnitude (Table 5 and 6) which are more common in East Asia than in the Sahel region. A high variability of PM_{10} values, especially for visibilities lower than 10 km (see Figure 4).

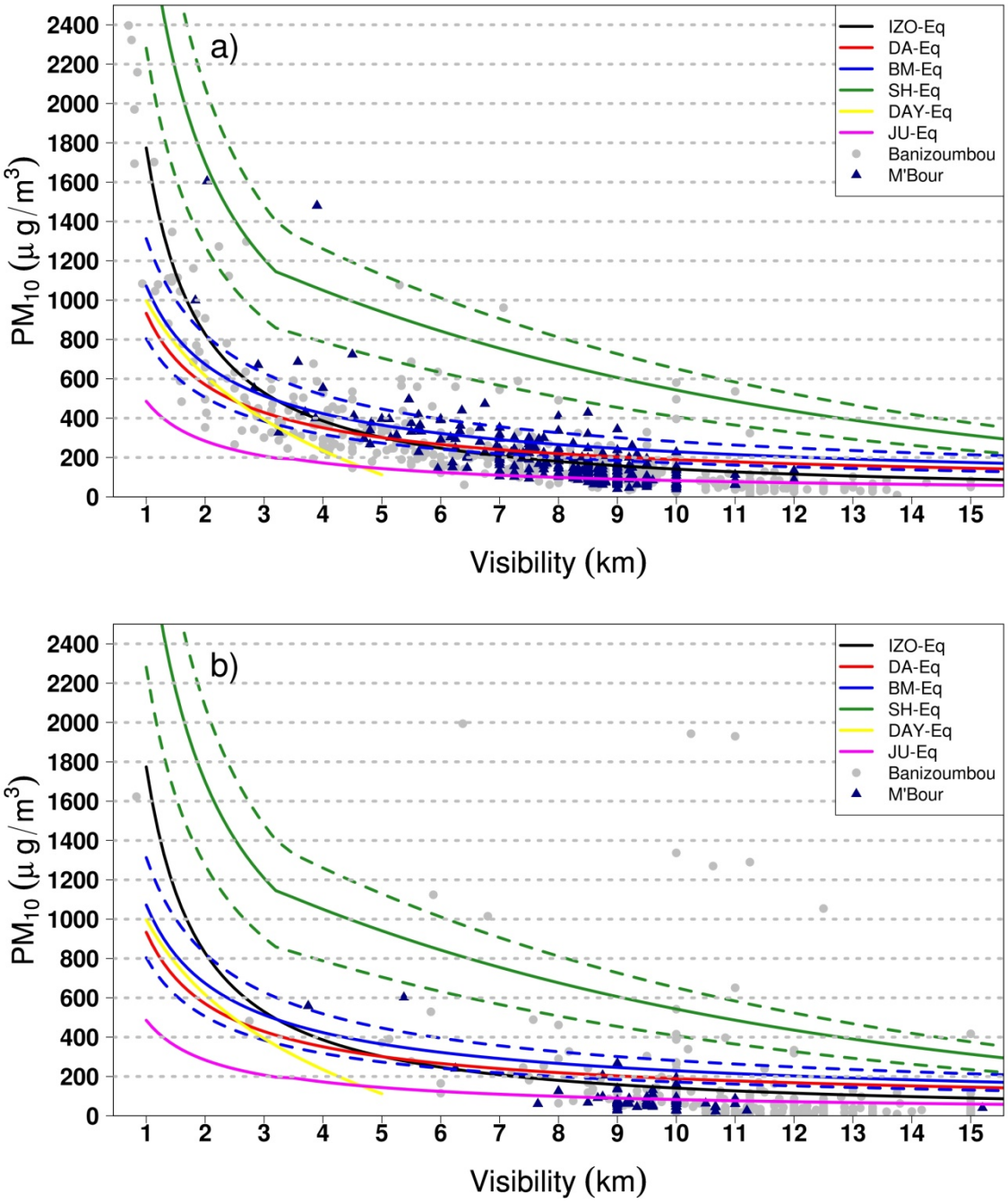

***Figure 4**. PM_{10} daily means ($\mu g/m^3$) versus visibility daily means (km) for each AMMA site during the dry (a) and wet (b) seasons for the period 2006-2008. Banizoumbou and M'Bour are represented by grey dots and blue triangles, respectively. Lines represent the estimated PM_{10} by IZO-Eq (black), DA-Eq (red), BM-Eq (blue), SH-Eq (green), DAY-Eq (yellow) and JU-Eq (pink). Since BM-Eq and SH-Eq provide TSP, the estimated values are converted to PM_{10} using an averaged TSP/PM_{10} ratio of 0.80 obtained at Banizoumbou station. These lines are confined within the dashed lines computed with the minimum (0.60) and maximum (0.98) PM_{10}/TSP values, respectively.*

During the dry season, the daily mean visibility of both AMMA stations was around 8 km (see Table 5). IZO-Eq is in good agreement with NMMB/BSC-Dust model and with observed PM10 concentrations at M'Bour and Banizoumbou stations, showing a good performance. We must emphasize the fact that, although IZO-Eq was obtained at Izaña

Observatory under conditions such that the maximum PM_{10} was just over 300 μg/m^3, and visibility was always above 4 km, presents excellent performance for high dust concentrations (PM_{10}> 1000 μg/m^3) and visibility ranges well below 4 km.
NMMB/BSC-Dust shows a significant scatter and overestimation, especially at Banizoumbou station. In order to compare the behavior of IZO-Eq with the other equations, we performed a detailed analysis dividing the datasets into three ranges of visibility: < 4 km, 4-10 km, and > 10 km (not shown here for the sake of brevity) for the dry season. For visibility < 4km, there is a reasonably good agreement between IZO-Eq, BM-Eq and DAY-Eq, and in-situ observations. SH-Eq significantly overestimates, while DA-Eq underestimates slightly, and Eq-JU significantly underestimates.

In Figure 5, IZO-Eq shows a rather good performance while DA-Eq tends to overestimate. The overall underestimation of DAY-Eq (MB < -64 μg/m^3 for both AMMA sites) might be explained by the fact that it was obtained with very low visibilities (≤ 5 km). This agrees with the fact that DAY-Eq shows the best performance for visibility < 4 km, with similar results to those of IZO-Eq. For visibility ranges between 4 and 10 km we find a good agreement between IZO-Eq and observations, a slight underestimation of JU-Eq, slight overestimation of DA-Eq and BM-Eq, and significant overestimation, again, of SH-Eq. For visibility ranges higher than 10 km, JU-Eq is the equation with the best results, followed by IZO-Eq, with a clear overestimation of the rest of the equations.

Table 5. *Statistics scores (MB, MNMB, FGE, RMSE and r) for each empirical equation and for surface dust concentrations from NMMB/BSC-Dust at M'Bour and Banizoumbou stations for the dry season (October - April 2006-2008). Median, Mean and standard deviation for visibility, and observed/estimated/simulated PM_{10}. Since BM-Eq and SH-Eq provide TSP, the estimated values are converted to PM_{10} using an averaged TSP/PM_{10} ratio of 0.80 obtained at Banizoumbou station.*

	Median	**Mean**	**SD**	**MB**	**MNMB**	**FGE**	**RMSE**	**r**	**n**
M'Bour									
Observed PM_{10} (μg/m^3)	**141**	**186**	**167**	…	…	…	…	…	…
Visibility (km)	**8.5**	**8.11**	**1.6**	…	…	…	…	…	…
NMMB/BSC-Dust	58	126	159	-60	-0.68	0.83	185	0.42	296
IZO-Eq	169	192	82	6	0.19	0.39	110	0.82	296
DA-Eq	211	225	49	39	0.37	0.50	135	0.82	296
BM-Eq	256	273	58	87	0.54	0.50	150	0.82	296
SH-Eq	736	781	160	595	1.31	1.31	603	0.81	296
DAY-Eq	414	443	152	-176	-0.22	0.31	185	0.62	17
JU-Eq	92	100	26	-87	0.39	0.49	170	0.82	296
Banizoumbou									
Observed PM_{10} (μg/m^3)	**129**	**230**	**334**	…	…	…	…	…	…
Visibility (km)	**9**	**8.11**	**3.03**	…	…	…	…	…	…
NMMB/BSC-Dust	150	286	364	56	0.12	0.57	329	0.57	622
IZO-Eq	158	258	291	28	0.33	0.45	190	0.83	622
DA-Eq	203	256	141	26	0.46	0.60	232	0.83	622
BM-Eq	246	308	162	78	0.62	0.60	233	0.83	622

SH-Eq	697	848	448	618	1.32	1.33	669	0.82	622
DAY-Eq	506	582	249	-64	0.05	0.29	439	0.72	115
JU-Eq	88	117	76	-113	-0.28	0.51	297	0.83	622

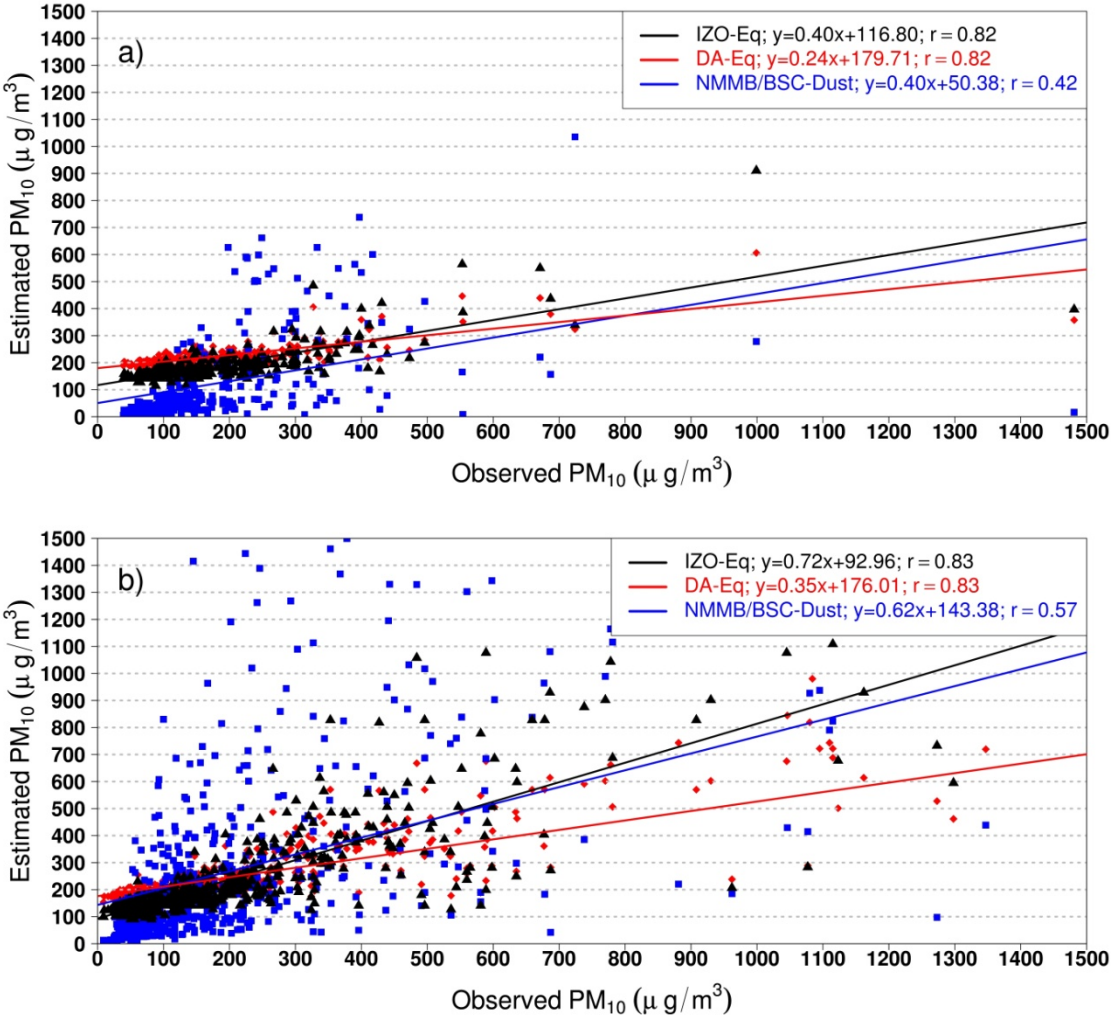

***Figure 5**. Scatter plot of observed PM_{10} daily means versus estimated PM_{10} daily means at M'Bour (a) and Banizoumbou (b) during the dry season for IZO-Eq (black triangles), DA-Eq (red diamonds) and NMMB/BSC-Dust surface dust concentration (blue dots). Lines correspond to the observed PM_{10} / estimated PM_{10} best fits for IZO-Eq (black), DA-Eq (red) and NMMB/BSC-Dust (blue).*

During the wet season, high values of PM_{10} coincide with high visibilities (Figure 4), which mostly correspond to observations at Banizoumbou station. The empirical equations mostly overestimate, being IZO-Eq the one which shows the best performance. IZO-Eq behaves well at Banizoumbou, and JU-Eq shows an excellent agreement with observations at M'Bour. The highest differences between estimated and

observed dust concentrations are provided by SH-Eq with a RMSE $\geq$ 514 $\mu g/m^3$ (Table 6). The empirical equations showed a high correlation ($r \geq 0.78$) at M'Bour. However, at Banizoumbou station the empirical equations showed relatively low correlation ($r \leq 0.45$), coincident with reported visibilities $\geq$ 10 km. Above 10 km visibility the empirical equations show a flat behavior with low PM_{10} variability (see Figure 4-b), indicating that 10 km is the upper limit, above which the empirical equations are not valid. IZO-Eq and DA-Eq tend to overestimate the low PM_{10} observations at each AMMA station (see Figure 6). However, a larger underestimation is observed at Banizoumbou (see Table 6 and Figure 6). This significant underestimation is related to the strong influence of local dust episodes during the MCS activity, which produce high PM_{10} records at Banizoumbou, but they are not registered by the nearby Synop stations. This apparent contradiction is explained by the fact that in the wet season the monsoon favors strong local dust events associated to MSC activity, which occur preferably during the night period and early morning hours (*Bou Karam et al. 2009; Marticorena et al. 2010*), while progressive dust removal and clearing up of the atmosphere takes place during daylight period at the lowermost levels (*Cavalieri et al. 2010*), resulting in relatively high visibility daily means since they are obtained with observations performed at daytime hours (9, 12, 15 and 18 UTC). For this reason we record a very low visibility/PM_{10} correlation at Banizoumbou station, and a clear underestimation during this season. Meanwhile, NMMB/BSC-Dust also underestimated during this season.

Understanding the causes that account for differences in results from the analyzed equations is a very complex task since we are comparing experimental equations that have been determined using different methodologies. Although this is outside the scope of this article, we can point out the most important factors in these equations that could explain the differences found between them under different conditions of visibility and dust content. Some of the equations (DA-Eq) establish the relationship between visibility and aerosol mass concentration indirectly using experimental measurements of aerosol turbidity with suphotometers, while others establish a direct relationship (IZO-Eq, BM-Eq, SH-Eq, DAY-Eq, JU-Eq). Some equations use PM_{10} data measured in the same synoptic stations where visibility is reported (IZO-Eq, DAY-Eq, JU-Eq), but other equations use data from PM_{10} or TSP sites and meteorological stations that are few kilometers away (DA-Eq, BM-Eq, SH-Eq), so that during certain events they might not sample the same air masses. On the other hand, the visibility ranges used are not the same for all stations. Some stations use visibility measurements performed with automated sensors (JU-Eq), which can be very different from those reported by human observers. The latter are subject, in turn, to subjective errors in estimating distances, as well as to protocols that may be different in each country, especially regarding the criteria of maximum range of visibility reported. In addition, not all stations use the same physical parameters related to aerosol mass concentration. Some of them used PM_{10} (IZO-Eq, DA-Eq, DAY-Eq, and JU-Eq) and others, TSP (BM-Eq and SH-Eq). Moreover, some equations were obtained without taking into account any criteria to separate the contribution of other aerosols, for example, those from biomass burning (BM-Eq), or to discard the events with high moisture content (SH- Eq). All this wide variety of factors has different impacts in the estimated PM_{10}, which depend, in turn, on the atmospheric aerosol content and visibility range.

Table 6. *Statistics scores (MB, MNMB, FGE, RMSE and r) for each empirical equation and for surface dust concentrations from NMMB/BSC-Dust at M'Bour and Banizoumbou stations for the wet season (May - September 2006-2008). Median, Mean and standard deviation for visibility, and observed/estimated/simulated PM_{10}. Since BM-Eq and SH-Eq provide TSP, the estimated values are converted to PM_{10} using an averaged TSP/PM_{10} ratio of 0.80 obtained at Banizoumbou station.*

	Median	**Mean**	**SD**	**MB**	**MNMB**	**FGE**	**RMSE**	**r**	**n**
M'Bour									
Observed PM_{10} ($\mu g/m^3$)	**66**	**90**	**94**	…	…	…	…	…	…
Visibility (km)	**9.5**	**9.46**	**1.3**	…	…	…	…	…	…
NMMB/BSC-Dust	21	35	53	-55	-0.97	0.99	77	0.87	74
IZO-Eq	149	155	38	65	0.69	0.75	92	0.82	74
DA-Eq	196	199	26	109	0.90	0.94	132	0.82	74
BM-Eq	237	241	31	151	1.04	0.94	167	0.82	74
SH-Eq	660	670	105	580	1.57	1.57	583	0.78	74
DAY-Eq	…	…	…	…	…	…	…	…	1
JU-Eq	85	86	13	-4	0.19	0.42	83	0.82	74
Banizoumbou									
Observed PM_{10} ($\mu g/m^3$)	**49**	**126**	**271**	…	…	…	…	…	…
Visibility (km)	**11.25**	**11.18**	**2.13**	…	…	…	…	…	…
NMMB/BSC-Dust	62	73	57	-53	0.05	0.62	270	0.20	311
IZO-Eq	124	137	122	11	0.71	0.93	249	0.40	311
DA-Eq	175	183	58	57	0.93	1.10	257	0.43	311
BM-Eq	212	220	67	94	1.05	1.10	266	0.44	311
SH-Eq	544	570	216	444	1.50	1.54	514	0.45	311
DAY-Eq	…	…	…	…	…	…	…	…	3
JU-Eq	74	78	31	-48	0.31	0.75	263	0.43	311

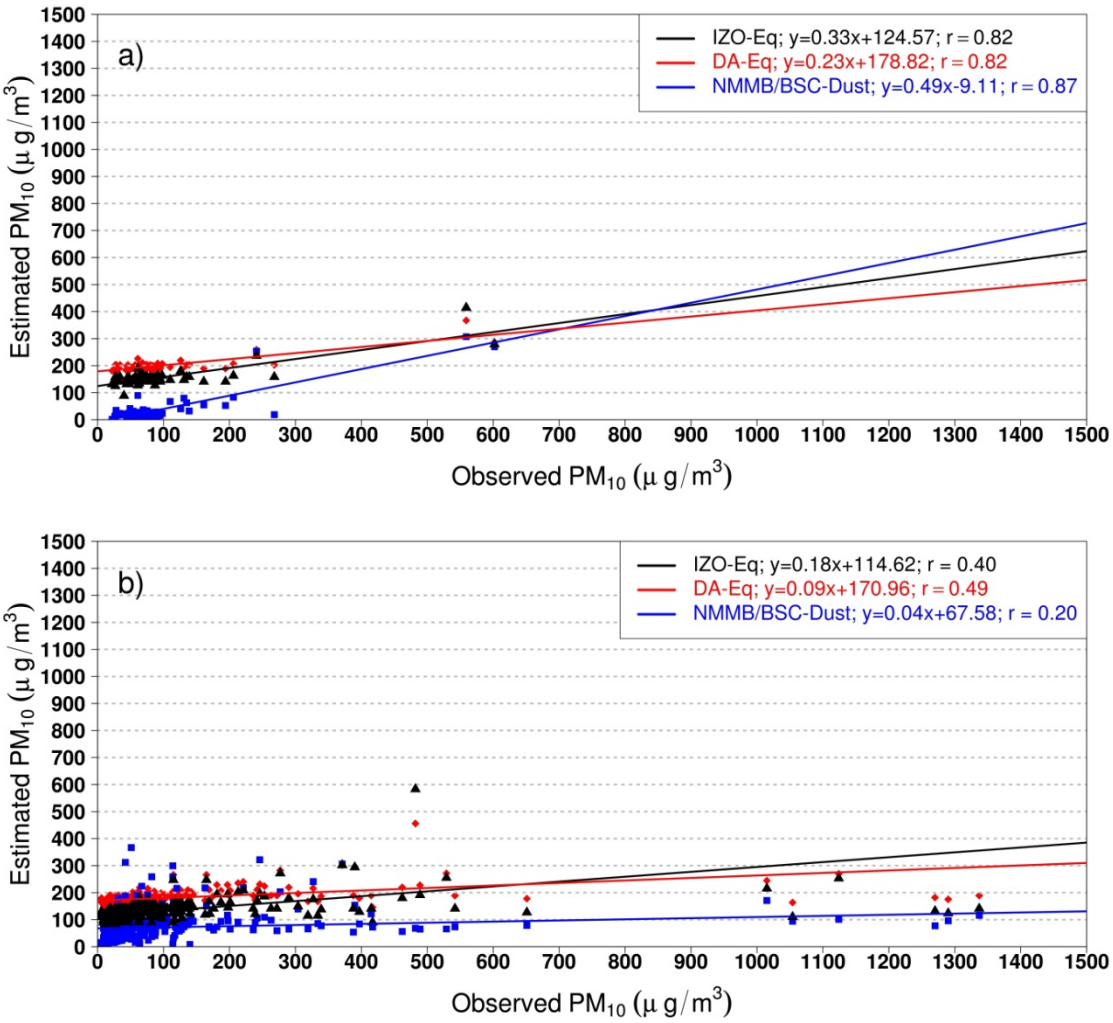

***Figure 6**. Scatter plot of observed PM_{10} daily means versus estimated PM_{10} daily means at M'Bour (a) and Banizoumbou (b) during the wet season for IZO-Eq (black triangles), DA-Eq (red diamonds) and NMMB/BSC-Dust surface dust concentration (blue dots). Lines correspond to the observed PM_{10} / estimated PM_{10} best fits for IZO-Eq (black), DA-Eq (red) and NMMB/BSC-Dust (blue).*

3.4 Estimation of PM_{10} spatial distribution over Northern Africa

Spatial maps of estimated PM_{10} from visibility observations over Northern Africa have been produced for the periods corresponding to the dry and wet seasons in the Sahel region. A large number of SYNOP stations are operational in Northern Africa. However, not all of them report visibility every three hours. SYNOP stations with less than 100 SYNOP observations for the entire period have been excluded from the analysis. All significant observations with the present weather codes 01-03, 05-09, 30-35 and 98 are considered.

IZO-Eq is used to convert visibility observations to PM_{10} concentrations. The Kriging method with spherical semivariogram model is used to perform a seasonal averaged map of estimated PM_{10}.Visibility data from 176 SYNOP stations located in Northern Africa were used to compute the spatial PM10 distributions. Regions with significant gaps of SYNOP stations were masked (see Figure 7-1).

The spatial distributions of seasonal mean PM_{10} concentrations estimated from visibility observations, simulated dust concentration from NMMB/BSC-Dust and AOD from MODIS from, for October-April 2006-2008, and for May-September 2006-2008, respectively, are shown in Figure 7. In Northern Africa, the Bodélé Depression in Chad (region A), northern part of Nigeria and the southern Niger (region B), Tunisia and Northeast Algeria (region C) Mali, Mauritania, and Western Sahara (region D), the eastern Libyan desert and the Egyptian sources (region E) are the regions with the highest PM_{10} concentrations. Those regions correspond to the main dust-source regions identified by *Prospero et al.* (2002) and *Ginoux et al. (2012).*

Estimated PM_{10} and NMMB/BSC-Dust surface dust concentration maps show that the major dust sources are located over the Bodélé depression in Chad (region A in Figure 7), and the northern part of Nigeria and the southern Niger (region B in Figure 7) from October to April (2006-2008), in agreement with the averaged AOD from MODIS. NMMB/BSC-Dust reproduces the high dust concentrations over the Bodélé Depression in Chad (region A in Figure 7) observed by MODIS. PM_{10} estimated by IZO-Eq is lower than NMMB/BSC-Dust. A significant disagreement between AOD from MODIS and estimated PM_{10} is found in these regions from May to September, likely due to the fact that the dust layer is observed in upper levels while there is good horizontal visibility at ground (daily mean visibility 13.30 ± 3.0 km) and the scarcity of SYNOP observations in this region.

The dust area located at northwest of Tombouctou (in Mali, region C in Figure 7), which is an active source region all year long (*Prospero et al., 2002*), extending to areas of southeast Mauritania (region C in Figure 7) is well captured by both estimated PM_{10} and AOD from MODIS in both periods. However, NMBB/BSC-Dust shows surface dust concentration underestimation, mainly in summer period, partly because dust sources in Mali and Mauritania are omitted by the topographic preferential source used in the model (*Pérez et al. 2011*).

The area immediately south of Chotts region abutting the Atlas Mountains to the west and the region located between Tunisia and northeast Algeria (32-35ºN, 5–10 ºE) (region D (Figure 7) is well captured by estimated PM_{10}, NMMB/BSC- Dust surface dust concentrations and AOD from MODIS in the two study periods. This dust source region shows maximum activity from April to September (*Prospero et al., 2002*) which is modulating by the hydrological cycle in this region (*Mahowald et al., 2003; Guinoux et al., 2012*).

The main dust source areas located between the eastern Libyan and the Egyptian dust sources (region E in Figure 7) are underestimated by IZO-Eq and NMBB/BSC-Dust in comparison with AOD from MODIS. Particularly, the high dust area observed over the west bank of the Nile River affecting Cairo, with maximum values from March to October, is reproduced by the IZO-Eq, NMMB/BSC-Dust and MODIS. High dust distribution over south Gulf of Sidra (in Libya) and the Qattara Depression is observed similarly by the IZO-Eq, NMMB/BSC-Dust and MODIS. However, the estimated PM_{10} by IZO-Eq shows a significant underestimation, likely due to scarcity of SYNOP stations.

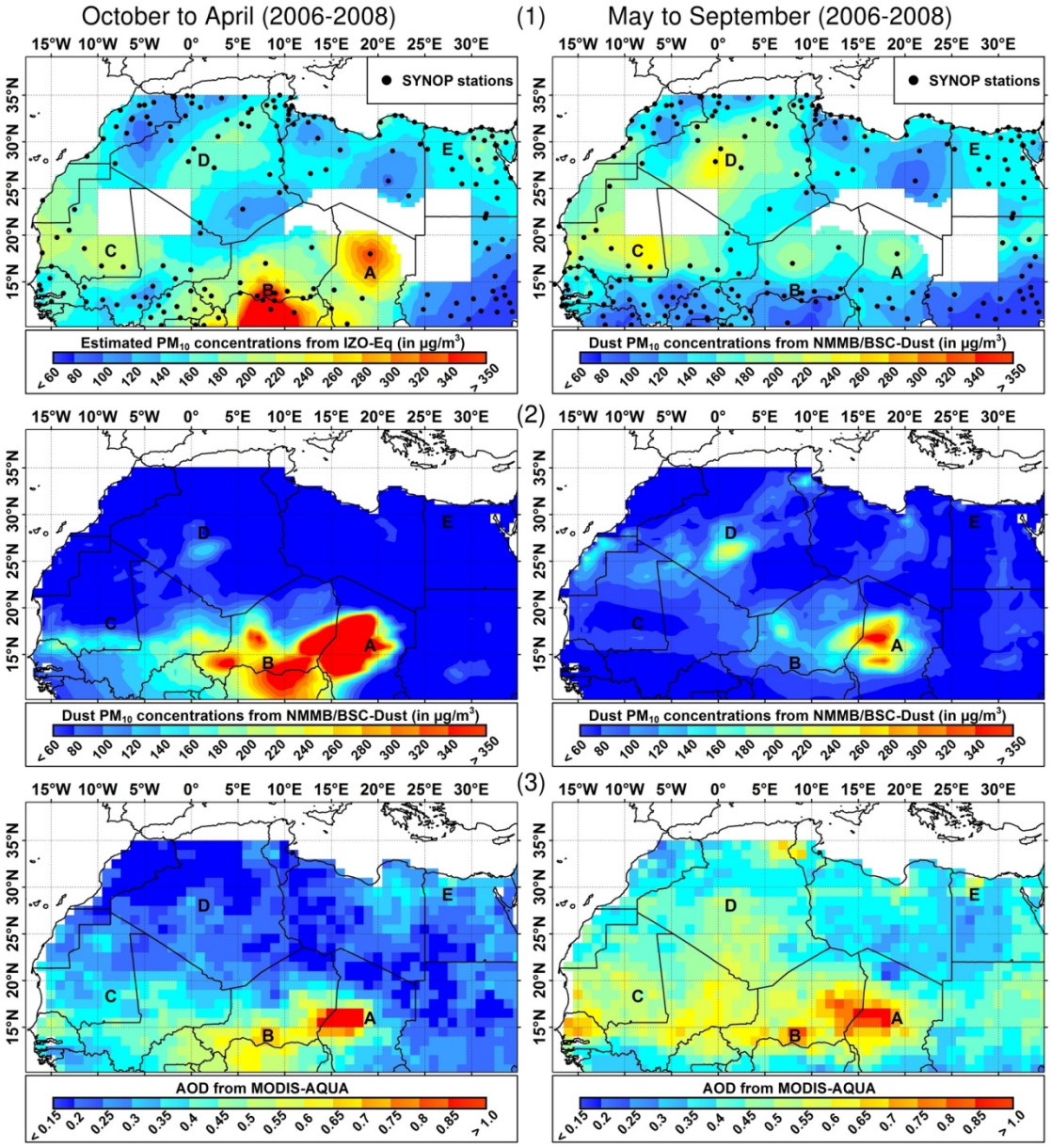

Figure 7*. Spatial distribution of PM10 (µg/m^3) from IZO-Eq (1), surface dust concentrations from NMMB/BSC-Dust (µg/m^3) (2), and AOD from MODIS (3), for October-April 2006-2008 (left column) and for May-September 2006-2008 (right column). Locations of the SYNOP stations used in the spatial interpolation are shown as black dots (1). A, the Bodélé Depression; B, northern part of Nigeria and southern Niger; C, Tunisia and northeast Algeria; D, Mali, Mauritania, and Western Sahara; E, the eastern Libyan desert and the Egyptian sources.*

4. Summary and conclusions

A new empirical equation relating horizontal visibility and PM_{10} concentration (referred as IZO-Eq) is obtained using observations at the Izaña high mountain GAW station under Saharan dust outbreaks. To derive the empirical equation, AERONET and SYNOP filters are applied to PM_{10}-horizontal visibility pairs of observations in order to ensure the visibility reduction is caused by suspended dust particles, discarding other weather conditions. This new empirical equation, IZO-Eq, is validated using visibility

and PM_{10} data recorded at two AMMA stations and the nearby synoptic stations in the Sahel region from January 2006 to December 2008. An analysis of AERONET data showed that clear sky conditions reported by SYNOP reports corresponded to background conditions normally characterized by the presence of haze. Therefore, visibility-PM_{10} pairs corresponding to clear sky conditions are used in the validation.

The IZO-Eq is compared against empirical equations reported in the literature and with surface dust concentrations from NMMB/BSC-Dust model. The IZO-Eq showed, in general, better scores than the other tested empirical equations during the wet and the dry seasons in the Sahel region from the comparison with measured PM_{10} and the NMMB/BSC-Dust model. The fact that the IZO-Eq is obtained with a large range of visibilities, from 4 to 75 km, might explained its good performance in the Sahel region during both seasons in comparison with the other tested empirical equations that mostly overestimated the observed values. In the range of high horizontal visibilities ($\geq$ 10 km), IZO-Eq showed a flat behavior with low variability of PM_{10}, indicating that 10 km is its limit of validity.

Additionally, the IZO-Eq is used to derive an estimated PM_{10} spatial distribution over Northern Africa, which was compared with NMMB/BSC-Dust surface dust concentrations and MODIS AOD from October to April and May to September 2006-2008. The IZO-Eq has demonstrated to be a useful tool for characterizing dust surface distribution over Northern Africa using interpolation methods. In fact, a high spatial consistency is observed with simulated PM_{10} concentrations from NMMB/BSC-Dust and AOD from MODIS. The estimated PM_{10} spatial distribution derived from visibility observations shows the main dust source regions previously identified by other authors (e.g., *Prospero et al. 2002*), such as the Bodélé depression in Chad, northern part of Nigeria and the southern Niger, Mali, Mauritania, and Western Sahara, Tunisia and Northeast Algeria, and eastern Libyan and Egyptian desert. The comparison of estimated PM_{10} and NMMB/BSC-Dust surface dust concentration with MODIS AOD shows a rather good agreement when the dust layer is observed at ground level.

To conclude, the present work demonstrates how the horizontal visibility reported by SYNOP stations might be useful for different applications as: 1) a first rough estimation of dust PM_{10} concentrations where there are no in-situ PM_{10}; 2) to estimate main features of atmospheric mineral dust geographical distribution and seasonal variations; and 3) to perform trend analysis of intense dust storms causing reduced visibility to less than 10 km.

5. Acknowledgements.

The present work was carried out in the framework of the MACC II project funded by the European Commission under the EU Seventh Research Framework Program (25 grant agreement number 283576), and as part of the activities of the World Meteorological Organization Sand and Dust Storm Warning Advisory and Assessment System Regional Center for Northern Africa, Middle East and Europe. Part of this study was performed within the frame of POLLINDUST project CGL2011-26259; Ministry of Economy and Competitiveness of Spain. The authors thank the AERONET program. MODIS data used in this paper were obtained from the Giovanni online data system, developed and maintained by the NASA GES DISC. NMMB/BSC-Dust simulations were performed on the Mare Nostrum supercomputer hosted by Barcelona

Supercomputing Center-Centro Nacional de Supercomputación (BSC-CNS) grant SEV-2011-00067 of Severo Ochoa Program, awarded by the Spanish Government. Based on a French initiative, AMMA was developed by an international scientific group and funded by a large number of agencies, especially from Africa, European Community, France, UK and USA. More information on the scientific coordination and funding is available on the AMMA International web-site: http://www.amma-international.org. The authors acknowledge B. Chatenet who managed the Sahelian Dust Transect from 2006 to 2012, J.L Rajot who largely participated to its installation and operation, and the local site managers in Niger (A. Maman and A. Zakou, IRD, Niamey), Mali (M. Coulibaly and I. Koné, IER, Cinzana) and Senegal (A. Diallo and T. NDiaye, IRD, M'Bour) for their efforts in the maintenance of the stations and for providing high-quality data.

6. References.

Alonso-Pérez, S., Cuevas, E., Querol, X., Viana, M., and Guerra, J., 2007. Impact of the Saharan dust outbreaks on the ambient levels of total suspended particles (TSP) in the marine boundary layer (MBL) of the Subtropical Eastern North Atlantic Ocean, Atmos. Environ., 41, 9468–9480.

Alonso-Pérez, S., Cuevas, E., Pérez, C., Querol, X., Baldasano, J.M, Draxler, R., and de Bustos, J., 2011. Trend changes of African airmass intrusions in the marine boundary layer over the subtropical Eastern North Atlantic region in winter, Tellus B, 63B, 255–265.

Basart, S., Pérez, C., Cuevas, E., Baldasano, J.M., Gobbi, G.P., 2009. Aerosol characterization in Northern Africa, Northeastern Atlantic, Mediterranean Basin and Middle East from direct-sun AERONET observations. Atmos. Chem. Phys., 9, 8265-8282.

Balkanski, Y., Schulz, M., Claquin, T., and Guibert, S., 2007. Reevaluation of Mineral aerosol radiative forcings suggests a better agreement with satellite and AERONET data, Atmos. Chem. Phys., 7, 81–95, doi:10.5194/acp-7-81-2007.

Ben Mohamed, A., Frangi, J.P., Fontan, J., Druilhet, A., 1992. Spatial and temporal variations of atmospheric turbidity and related parameters in Niger. J. Appl. Meteorol., 31, 1286–1294.

Bou Karam, D, Flamant, C, Knippertz, P, Reitebuch, O, Pelon, J, Chong, M, Dabas, A., 2008. Dust emissions over the Sahel associated with the West African monsoon intertropical discontinuity region: A representative case-study. Q. J. R. Meteorol. Soc. 134: 621–634.

Bou Karam D., Flamant C., Tulet P., Chaboureau J.-P., Dabas A., Todd M.C., 2009. Estimate of Sahelian dust emissions in the intertropical discontinuity region of the West African Monsoon. J. Geophys. Res., 114, D13106, doi:10.1029/2008JD011444.

Cabello, M., Orza J.A.G., Barrero M.A., Gordo E., Berasaluce A., Cantón L., Dueñas C., Fernández M.C., and Pérez, M., 2012. Spatial and temporal variation of the impact of an extreme Saharan dust event. J. Geophys. Res. Vol 117, D11204, doi:10.1029/2012JD017513.

Cavalieri, O., Di Donfrancesco, G., Cairo, F., Fierli, F., Snels, M., Viterbini, M., Cardillo, F., Chatenet, B., Formenti, P., Marticorena, B., and Rajot, J.L., 2010. Variability of aerosol vertical distribution in the Sahel, Atmos. Chem. Phys., 10, 12005–12023. doi:10.5194/acp-10-12005-201.

Chepil W, Woodruff N., 1957. Sedimentary characteristics of dust storms. II. Visibility and dust concentration. American Journal of Science 255: 104–114.

Cuevas, E., Pérez, C., Baldasano, J.M., Camino, C., Alonso-Pérez, S., and Basart, S., 2011. MACC O-INT WP3.1.Meningitis linked to mineral dust transport in the Sahel, Monitoring Atmospheric Composition and Climate, Second delivery Report.

D'Almeida, G.A., 1986. A model for Saharan dust transport. J. Clim. Appl. Meteorol., 25 (7), 903–916.

Dayan, U., Ziv, B., Shoob, T., and Enzel, Y., 2008. Suspended dust over southeastern Mediterranean and its relation to atmospheric circulations. Int. J. Climatol. Volume 28, Issue 7, pages 915–924, 15 June. DOI: 10.1002/joc.1587.

Desboeufs, K., Journet, E., Rajot, J.L., Chevaillier, S., Triquet, S., Formenti, P., and Zakou, A., 2010. Chemistry of rain events in West Africa: evidence of dust and biogenic influence in convective systems, Atmos. Chem. Phys., 10, 9283–9293, doi:10.5194/acp-10-9283-2010.

De Paepe, B., and Dewitte, S., 2009. Dust Aerosol Optical Depth Retrieval over a Desert Surface Using the SEVIRI Window Channels. J. Atmos. Oceanic Technol., 26, 704–718. Doi: http://dx.doi.org/10.1175/2008JTECHA1109.1.

Díaz, J., Tobías A., and Linares, C., 2012. Saharan dust and association between particulate matter and case-specific mortality: a case crossover analysis in Madrid (Spain), Environmental Health, 11:11.

Engelstaedter, S., Tegen, I., Washington, R., 2006. North African dust emissions and transport. Earth Sci. Rev. 79 (1–2), 73–100.

Engelstaedter, S., and Washington ,R., 2007. Temporal controls on global dust emissions: The role of surface gustiness, Geophys. Res. Lett., 34, L15805, doi:10.1029/2007GL029971.

Flamant, C., Chaboureau, J.-P., Parker, D.J., Taylor, C. M., Cammas, J.-P., Bock, O., Timouck, F., and Pelon, J., 2007. Airborne observations of the impact of a convective system on the planetary boundary layer thermodynamics and aerosol distribution in the inter-tropical discontinuity region of the West African Monsoon, Q. J. Roy. Meteorol. Soc., 133, 1175–1189, doi:10.1002/qj.97.

Flamant, C., Lavaysse, C., Todd, M.C., Chaboureau, J.-P., and Pelon, J., 2009. Multi-platform observations of a representative springtime case of Bodélé and Sudan dust emission, transport and scavenging over West Africa, Q. J. Roy. Meteorol. Soc., 135(639), 413–430.

Formenti, P., Rajot, J.L., Desboeufs K., Saïd, F., Grand, N., Chevaillier, S. and Schmechtig, S., 2011. Airborne observations of mineral dust over western Africa in the summer Monsoon season: spatial and vertical variability of physico-chemical and optical properties. Atmos. Chem. Phys., 11, 6387–6410. doi:10.5194/acp-11-6387-2011.

Ginoux, P., Prospero, J.M., Gill, T.E., Hsu, N.C., and Zhao, M., 2012. Global scale attribution of anthropogenic and natural dust sources and their emission rates based on MODIS Deep Blue aerosol products, Reviews of Geophysics, 50, doi: 10.1029/2012RG000388.

Griffin, D.W., and C.A., Kellogg. 2004. Dust storms and their impact on ocean and human health: Dust in Earth's atmosphere. EcoHealth 1: 284-295.

Griffin, D.W., 2007. Atmospheric Movement of Microorganisms in Clouds of Desert Dust and Implications for Human Health, doi: 10.1128/CMR.00039-06, Clin. Microbiol. Rev., 20, 3, 459-477.

Gyan, K., Henry, W., Lacaille, S., Laloo, A., Lamsee-Ebanks, C., McKay, S., Antoine, R.M., and Monteil, M.A., 2005. African dust clouds are associated with increased pediatric asthma accident and emergency admissions on the Caribbean island of Trinidad, International Journal of Biometeorology, 49, 371-376.

Hamidi, M., Kavianpour, M. R., & Shao, Y., 2013. Synoptic analysis of dust storms in the Middle East. Asia-Pacific Journal of Atmospheric Sciences, 49(3), 279-286.

Haustein K., Pérez, C., Baldasano, J.M., Jorba, O., Basart, S., Miller, R.L., Janjic, Z., Black, T., Nickovic, S., Todd, M.C., and Washington R., 2012. Atmospheric dust modeling from meso to global scales with the online NMMB/BSC-Dust model–Part 2: Experimental campaigns in Northern Africa. Atmos. Chem. Phys., 12, 2933–2958, doi:10.5194/acp-12-2933.

Heinold, B., Tegen, I., Schepanski, K., and Hellmuth, O., 2008 Dust Radiative Feedback on Saharan Boundary Layer Dynamics and Dust Mobilization. Geophys. Res. Lett. 35, L20817, doi:10.1029/2008GL035319.

Holben, B.N., Eck, T.F., Slutsker, I., Tanré, D., Buis, J.P., Setzer, A., Vermote, E., Reagan, J., Kaufman, Y., Nakajima, T., Lavenu, F., Jankowiak, I. and Smirnov, A., 1998. AERONET: A Federated Instrument Network and Data Archive for Aerosol Characterization". Rem. Sens. Environ. 66: 1-16.

Hoose, C., Lohmann, U., Erdin, R., and Tegen, I., 2008. The global influence of dust mineralogical composition on heterogeneous ice nucleation in mixed-phase clouds. Environmental Research Letters, 3(2), 025003, doi:10.1088/1748-9326/3/2/025003.

Hsu, N.C., Tsay, S.-C., King, M.D., and Herman, J.R., 2004. Aerosol properties over bright-reflecting source regions. IEEE Trans. Geosci. Remote Sens., 42 (3), 557–569.

Hsu, N C., Gautam, R., Sayer, A. M., Bettenhausen, C., Li, C., Jeong, M. J., Tsay, S.-C., and Holben, B.N., 2012. Global and regional trends of aerosol optical depth over land and ocean using SeaWiFS measurements from 1997 to 2010, Atmos. Chem. Phys., 12, 8037-8053, doi:10.5194/acp-12-8037-2012.

Huneeus, N., Schulz, M., Balkanski, Y., Griesfeller, J., Prospero, J., Kinne, S., Bauer, S., Boucher, O., Chin, M., Dentener, F., Diehl, T., Easter, R., Fillmore, D., Ghan, S., Ginoux, P., Grini, A., Horowitz, L., Koch, D., Krol, M.C., Landing, W., Liu, X., Mahowald, N., Miller, R., Morcrette, J.-J., Myhre, G., Penner, J., Perlwitz, J., Stier, P., Takemura, T., and Zender, C.S., 2011. Global dust model intercomparison in AeroCom phase I, Atmos. Chem. Phys., 11, 7781–7816, doi:10.5194/acp-11-7781-2011.

IPCC, Intergovernmental Panel on Climate Change (2007). Climate Change 2007: The Physical Basis. Contribution of the Working Group I to the Fourth Assessment Report of the Intergovernmental Panel on Climate Change. Edited by Solomon, S., Qin, D., Manning, M., Chen, Z., Marquis, M., Averyt, K.B., Tignor, M., Miller, H.L. Cambridge University Press, Cambridge, United Kingdom.

IPCC, Intergovernmental Panel on Climate Change (2014). Climate Change 2013: The Physical Science Basis. Cambridge University Press, Cambridge, United Kingdom. https://www.ipcc.ch/report/ar5/wg1/.

Janicot, S., Thorncroft, C.D., Ali, A., Asencio, N., Berry, G., Bock, O., Bourles, B., Caniaux, G., Chauvin, F., Deme, A., Kergoat, L., Lafore, J.-P., Lavaysse, C., Lebel, T., Marticorena, B., Mounier, F., Nedelec, P., Redelsperger, J.-L., Ravegnani, F., Reeves, C.E., Roca, R., de Rosnay, P., Schlager, H., Sultan, B., Tomasini, M., Ulanovsky, A., and ACMAD forecasters team., 2008. Large-scale overview of the summer monsoon over West Africa during the AMMA field experiment in 2006, Ann. Geophys., 26, 2569– 2595, doi:10.5194/angeo-26-2569-2008.

Jickells, T. D., An, Z.S., Andersen, K.K., Baker, A.R., Bergametti, G., Brooks, N., Cao, J.J., Boyd, P.W., Duce, R.A., Hunter, K.A., Kawahata, H., Kubilay, N., laRoche J., Liss, P.S., Mahowald, N., Prospero, J.M., Ridgwell, A.J., Tegen, I., and Torres, R.,

2005. Global iron connections between desert dust, ocean biogeochemistry, and climate, Science, 308, 67–71. DOI:10.1126/science.1105959.

Jugder, D., Shinoda, M., Kimura, R., Batbold, A., and Amarjargal, D., 2014. Quantitative analysis on windblown dust concentrations of PM10 (PM2.5) during dust events in Mongolia, Aeolian Research, Vol. 14, 3-13, ISSN 1875-9637, http://dx.doi.org/10.1016/j.aeolia.2014.04.005.

Klein, H., Nickovic, S., Haunold, W., Bundke, U., Nillius, B., Ebert, M., Weinbruch, S., Schuetz, L., Levin, Z., Barrie, L.A., and Bingemer, H., 2010. Saharan dust and ice nuclei over Central Europe, Atmos. Chem. Phys., 10, 10211-10221, doi:10.5194/acp-10-10211-2010.

Klose, M., Shao, Y., Karremann, K., Fink, A.H., 2010. Sahel dust zone and synoptic background. Geophys. Res. Lett. Vol. 37, L09802, doi:10.1029/2010GL042816.

Lebel, T., Parker, D.J., Flamant, C., Bourlès, B., Marticorena, B., Mougin, E., Peugeot, C., Diedhiou, A., Haywood, J.M., Ngamini, J.B., Polcher, J., Redelsperger, J.-L., and Thorncroft, C.D., 2010. The AMMA field campaigns: multiscale and multidisciplinary observations in the West African region, Q. J. Roy. Meteorol.Soc., 136(S1), 8–33.

Levy, R.C., Remer, L.A., Kleidman, R.G., Mattoo, S., Ichoku, C., Kahn, R. and Eck, T.F. (2010). Global Evaluation of the Collection 5 MODIS Dark-Target Aerosol Products over Land. Atmos.Chem. Phys. 10:10399–10420.

Leys, J.F., McTainsh, G.H., Shao, Y., Tews, E.K., 2002. Testing of region wind erosion models for environmental auditing. In: Lee, J.A., Zobeck, T.M. (Eds.), Fifth International Conference On Aeolian Research, Publication. No. 02-2, Texas Tech University, Lubbock, Texas, USA, 22–25 July. (International Centre for Arid and Semi-arid Lands Studies, Texas Tech University, USA), pp. 168-172.

Maher, B.A., Prospero, J.M., Mackie, D., Gaiero, D., Hesse, P., Balkanski, Y., 2010. Global connections between aeolian dust, climate and ocean biogeochemistry at the present day and at the last glacial maximum. 99, 1–2, 61–97, doi:10.1016/j.earscirev.2009.12.001.

Mahowald, N.M., Bryant R.G., del Corral J., and Steinberger L., 2003. Ephemeral lakes and desert dust sources, Geophys. Res. Lett., 30, 1074, doi:10.1029/2002GL016041.

Mahowald, N.M., Ballantine, J.A., Feddema, J., Ramankutty, N., 2007. Global trends in visibility: implications for dust sources. Atmos. Chem. Phys. 7 3309-3339.

Marticorena, B., Chatenet, B., Rajot, J.L., Traoré, S., Coulibaly, M., Diallo, A., Koné, I., Maman, A., NDiaye, T., Zakou, A., 2010. Temporal variability of mineral dust concentrations over West Africa: analyses of a pluriannual monitoring from the AMMA Sahelian Dust Transect. Atmos. Chem. Phys., 10, 8899–8915.

Morcrette, J.-J., Boucher, O., Jones, L., Salmond, D. Bechtold, P. Beljaars, A. Benedetti, A., Bonet, A., Kaiser, J.W., Razinger, M., Schulz, M., Serrar, S., Simmons, A.J., Sofiev, M., Suttie, M., Tompkins, A.M., and Untch A., 2009. Aerosol analysis and forecast in the ECMWF Integrated Forecast System. Part I: Forward modelling, J. Geophys. Res., 114, D06206, doi:10.1029/2008JD011235.

Nicholson, E.S., 2009. A revised picture of the structure of the ‘‘monsoon’’ and land ITCZ over West Africa. Clim Dyn. 32:1155–1171DOI 10.1007/s00382-008-0514-3

Nicholson, E.S., 2013. The West African Sahel: A Review of Recent Studies on the Rainfall Regime and Its Interannual Variability. ISRN Meteorology Volume 2013, Article ID 453521, http://dx.doi.org/10.1155/2013/453521.

Nickovic, S., Papadopoulos, A., Kakaliagou, O., and Kallos, G., 2001. Model for prediction of desert dust cycle in the atmosphere. J. Geophys. Res., 106, 18,113–18,129.

N'Tchayi Mbourou, G.N., Bertrand, J.J., Nicholson, S.E., 1997. The diurnal and seasonal cycles of wind-borne dust over Africa north of the equator. J. Appl. Meteorol., 36 (7), 868–882.

Ohde, T., and Siegel, H., 2012. Impacts of Saharan dust and clouds on photosynthetically available radiation in the area off Northwest Africa, Tellus B, 64, 17160, DOI: 10.3402/tellusb.v64i0.17160.

O'Neill, N., Eck, T., Smirnov, A., Holben, B. and Thulasiraman, S., 2003. Spectral discrimination of coarse and fine mode optical depth. J. Geophys. Res. Atmos, Vol. 108 (D17). ISSN 0148-0227.

Ozer, P, Laghdaf, M.B.O.M, Lemines, S.O.M, Gassani, J., 2006. Estimation of air quality degradation due to Saharan dust at Nouakchott, Mauritania, from horizontal visibility data. Water Air Soil Poll. 1–4:79–87. doi:10.1007/s11270-006-9152.

Patterson, E.M., Gillette, D.A., 1977. Measurements of visibility vs. mass concentration for airborne soil particles. Atmos. Environ. 11: 193–196.

Pérez, C., Nickovic, S., Pejanovic, G., Baldasano, J.M., and Ozsoy, E., 2006. Interactive Dust-radiation Modeling: A Step to improve Weather Forecast. J. of Geophys Res. 111, D16206, doi:10.1029/2005JD006717.

Pérez, C., Haustein, K., Janjic, Z., Jorba, O., Huneeus, N., Baldasano, J.M., Black, T., Basart, S., Nickovic, S., Miller, R.L., Perlwitz, J.P., Schulz, M., and Thomson, M., 2011. Atmospheric dust modeling from meso to global scales with the online NMMB/BSC-Dust model-Part 1: Model description, annual simulations and evaluation, Atmos. Chem. Phys., 11, 13001-13027, doi:10.5194/acp-11-13001.

Pérez, C., Stanton, M., Diggle, P., Trzaska, S., Hugonnet, S., Miller, R., Perlwitz, J.P., Baldasano, J.M., Cuevas, E., Ceccato, P., Yaka, P., and Thomson, M., 2014. Soil dust aerosols as predictors of seasonal meningitis incidence in Niger, Environ Health Perspect; DOI:10.1289/ehp.1306640 Prospero, J. M., Ginoux, P., Torres, O., Nicholson, S.E. and Gill, T.E. (2002). Environmental characterization of global sources of atmospheric soil dust identified with the nimbus 7 total ozone mapping spectrometer (TOMS) absorbing aerosol product. Rev. Geophys. 40(1), 1002.

Rajot, J.L., Formenti, P., Alfaro, S., Desboeufs, K., Chevaillier, S., Chatenet, B., Gaudichet, A., Journet, E., Marticorena, B., Triquet, S., Maman, A., Mouget, N., Zakou. A., 2008. AMMA dust experiment: An overview of measurements performed during the dry season special observation period (SOP0) at the Banizoumbou (Niger) supersite, J. Geophys. Res., 113, doi:10.1029/2008JD009906.

Ramanathan V., Crutzen P.J., Kiehl J.T., Rosenfeld D., 2001. Aerosols, Climate, and the Hydrological Cycle. Science 7, Vol. 294. no. 5549, pp. 2119 – 2124. DOI: 10.1126/science.1064034.

Rodríguez, S., González, Y., Cuevas, E., Ramos, R., Romero, P.M., Abreu-Afonso, J., and Redondas, A., 2009. Atmospheric nanoparticle observations in the low free troposphere during upward orographic flows at Izaña Mountain Observatory, Atmos. Chem. Phys., 9, 6319–6335, doi:10.5194/acp-9-6319-2009.

Rodríguez, S., Alastuey A., Alonso-Perez, S., Querol, X., Cuevas, E., Abreu-Afonso, J., Viana, M., Pérez, N., Pandolfi, M. and de la Rosa, J., 2011. Transport of desert dust mixed with North African industrial pollutants in the subtropical Saharan Air Layer. Atmos. Chem. Phys., 11, 6663–6685.

Rodríguez, S., Alastuey A., Querol X., 2012. A review of methods for long term in situ characterization of aerosol dust. Aeolian Res. 6 , 55–74.

Schroedter-Homscheidt, M., Oumbe, A., Benedetti, A., and Morcrette, J.-J., 2012. Aerosols for concentrating solar electricity production forecasts: requirement quantification and ECMWF/MACC aerosol forecast assessment. Bulletin of the American Meteorological Society, doi: http://dx.doi.org/10.1175/BAMS-D-11-00259.

Shao, Y., Wang L., 2003. A climatology of northeast Asian dust events. Meteorol. Z., 12, 187–196. J. Atmos, and Oceanic technology, Vol 26, 704-718.

Shao, Y., and Dong, C.H. 2006, A review on East Asian dust storm climate, modelling and monitoring, Global Planet. Change, 52, 1–22, doi:10.1016/j.gloplacha.2006.02.011.

Shao Y., Wyrwoll K.-H., Chappell, A., Huang, J., Lin, Z., McTainsh, G.H., Mikami, M., Tanaka, T.Y., Wang, X., Yoon, S., 2011. Dust cycle: An emerging core theme in Earth system science. Aeolian Res. 2 181–204.

Shi, Y., Zhang, J., Reid, J.S., Hyer, E.J., and Hsu, N.C., 2013. Critical evaluation of the MODIS Deep Blue aerosol optical depth product for data assimilation over North Africa. Atmos. Meas. Tech., 6, 949–969, 2013. doi:10.5194/amt-6-949-2013.

Stefanski, R., and Sivakumar, M.V.K., 2009. Impacts of Sand and Dust Storms on Agriculture and Potential Agricultural Applications of a SDSWS, IOP Conf. Ser.: Earth Environ. Sci., 7, 012016 doi:10.1088/1755-1307/7/1/012016.

Sterk, G., 2002. Causes, consequences and control of wind erosion in Sahelian Africa: A review, Land Degrad. & Dev., 14, 95– 108.

Sunnu, A., Afeti, G., and Resch, F., 2008, A long-term experimental study of the Saharan dust presence in West Africa, Atmospheric Research, Vol. 87, 1, 13–26.

Tegen, I., 2003. Modeling the mineral dust aerosol cycle in the climatesystem, Quaternary Sci. Rev., 22(18–19), 1821–1834.

Tews, E.K.,1996. Wind erosion rates from meteorological records in eastern Australia 1960–92. Thesis, Griffith University, Australia.

Thomson, M.C, Molesworth A.M., Djingarey, M.H., Yameogo, K.R., Belanger, F., Cuevas, L.E., 2006. Potential of environmental models to predict meningitis epidemics in Africa. Tropical Medicine & International Health 11(6), 781-788.

Todd, M.C., Bou Karam, D., Cavazos, C., Bouet, C., Heinold, B., Baldasano, J.M., Cautenet, G., Koren, I., Pérez, C., Solmon, F., Tegen, I., Tulet, P., Washington, R., and Zakey A., 2008. Quantifying uncertainty in estimates of mineral dust flux: An intercomparison of model performance over the Bodélé Depression, northern Chad. J. Geophys. Res., 113.

Toledano, C., Wiegner, M., Groß, S., Freudenthaler, V., Gasteiger, J. and co-authors., 2011. Optical properties of aerosol mixtures derived from sun-sky radiometry during SAMUM-2. Tellus B. 63(4), 635-648.

Torres, C., Cuevas, E., and Guerra, J.C., 2002. Caracterización de la capa de mezcla marítima y de la atmósfera libre en la región subtropical sobre Canarias. Asamblea Hispano Portuguesa de Geodesia y Geofisica, Valencia, Spain.

Uno, I., Wang, Z., Chiba, M., Chun, Y.S., Gong, S.L., Hara, Y., Jung, E., Lee, S.S., Liu, M., Mikami, M., Music, S., Nickovic, S., Satake, S., Shao, Y., Song, Z., Sugimoto, N., Tanaka, T., and Westphal, D.L., 2006. Dust model intercomparison (DMIP) study over Asia: Overview, J. Geophys. Res., 111(D12), D12213, doi:10.1029/2005JD006575.

Washington, R., Preston A., Todd M., 2003. Sea surface temperature influences on African rainfall variability, B Am. Meteorol. Soc. 84 (7): 899-900.

Wang, Y.Q., Zhang, X.Y., Gong, S. L. , Zhou, C.H. , Hu, X.Q. , Liu, H.L. , Niu, T. , and Yang, Y.Q., 2008. Surface observation of sand and dust storm in East Asia and its application in CUACE/Dust. Atmos. Chem. Phys., 8, 545-553.

WHO, WHO air quality guidelines global update 2005, Bonn, Germany, World Health Organization, 2005.

Yahi, H., Marticorena, B., Thiria, S., Chatenet, B., Schmechtig, C., Rajot, J.L., and Crepon M., 2013. Statistical relationship between surface PM10 concentration and aerosol optical depth over the Sahel as a function of weather type, using neural network methodology, J. Geophys. Res. Atmos., 118, 13,265–13,281, doi:10.1002/2013JD019465.